Ice sintering: Dependence of sintering force on temperature, load, duration, and particle size

Downloaded from: https://research.chalmers.se, 2026-04-05 19:38 UTC

Citation for the original published paper (version of record):

Bahaloo, H., Eidevåg, T., Gren, P. et al (2022). Ice sintering: Dependence of sintering force on temperature, load, duration, and particle size. Journal of Applied Physics, 131(2). http://dx.doi.org/10.1063/5.0073824

N.B. When citing this work, cite the original published paper.

research.chalmers.se offers the possibility of retrieving research publications produced at Chalmers University of Technology. It covers all kind of research output: articles, dissertations, conference papers, reports etc. since 2004. research.chalmers.se is administrated and maintained by Chalmers Library

(article starts on next page)

Journal of Applied Physics

Ice sintering: Dependence of sintering force on temperature, load, duration, and particle size

Cite as: J. Appl. Phys. **131**, 025109 (2022); https://doi.org/10.1063/5.0073824
Submitted: 04 October 2021 • Accepted: 24 December 2021 • Published Online: 12 January 2022

Hassan Bahaloo, Tobias Eidevåg, Per Gren, et al.

COLLECTIONS

This paper was selected as Featured

This paper was selected as Scilight

View Online Export Citation CrossMark

ARTICLES YOU MAY BE INTERESTED IN

Synthesis and structure of carbon-doped H_3S compounds at high pressure
Journal of Applied Physics **131**, 025902 (2022); https://doi.org/10.1063/5.0073499

Transducerless time domain reflectance measurement of semiconductor thermal properties
Journal of Applied Physics **131**, 025101 (2022); https://doi.org/10.1063/5.0069360

Atomistic simulation on the formation mechanism of bonding interface in explosive welding
Journal of Applied Physics **131**, 025903 (2022); https://doi.org/10.1063/5.0069720

AIP Publishing Applied Physics Reviews
Read. Cite. Publish. Repeat.
19.162
2020 IMPACT FACTOR*

© 2022 Author(s).

Journal of Applied Physics ARTICLE scitation.org/journal/jap

Ice sintering: Dependence of sintering force on temperature, load, duration, and particle size

Cite as: J. Appl. Phys. **131**, 025109 (2022); doi: 10.1063/5.0073824
Submitted: 4 October 2021 · Accepted: 24 December 2021 ·
Published Online: 12 January 2022

View Online Export Citation CrossMark

Hassan Bahaloo,[1,a)] Tobias Eidevåg,[2,3] Per Gren,[1] Johan Casselgren,[1] Fredrik Forsberg,[1] Per Abrahamsson,[4] and Mikael Sjödahl[1]

AFFILIATIONS

[1]Division of Experimental Mechanics, Luleå University of Technology, Luleå 97187, Sweden
[2]Department of Chemistry and Chemical Engineering, Chalmers University of Technology, SE-41296 Gothenburg, Sweden
[3]Contamination and Core CFD, Volvo Car Corporation, SE-405 31 Gothenburg, Sweden
[4]Technical Analysis, Fluid Mechanics, AFRY, Gothenburg 412 63, Sweden

[a)]**Author to whom correspondence should be addressed:** hassan.bahaloohoreh@ltu.se

ABSTRACT

We present experiments along with an approximate, semi-analytic, close-form solution to predict ice sintering force as a function of temperature, contact load, contact duration, and particle size during the primary stage of sintering. The ice sintering force increases nearly linear with increasing contact load but nonlinear with both contact duration and particle size in the form of a power law. The exponent of the power law for size dependence is around the value predicted by general sintering theory. The temperature dependence of the sintering force is also nonlinear and follows the Arrhenius equation. At temperatures closer to the melting point, a liquid bridge is observed upon the separation of the contacted ice particles. We also find that the ratio of ultimate tensile strength of ice to the axial stress concentration factor in tension is an important factor in determining the sintering force, and a value of nearly 1.1 MPa can best catch the sintering force of ice in different conditions. We find that the activation energy is around 41.4 KJ/mol, which is close to the previously reported data. Also, our results suggest that smaller particles are "stickier" than larger particles. Moreover, during the formation of the ice particles, cavitation and surface cracking is observed which can be one of the sources for the variations observed in the measured ice sintering force.

© 2022 Author(s). All article content, except where otherwise noted, is licensed under a Creative Commons Attribution (CC BY) license (http://creativecommons.org/licenses/by/4.0/). https://doi.org/10.1063/5.0073824

I. INTRODUCTION

Ice particles tend to stick together quickly since ice is almost always near its melting point.[1–3] Due to the sticking of ice particles, a pull-off force is required to separate them. This pull-off force is called sintering force.[2] A better understanding of ice sintering can help simulate snow behavior better,[4–6] understand ice friction and sliding,[7,8] and provide insight to the relevant physical and natural phenomena like snow avalanche.[9–11] Ice sintering studies are also helpful in fields related to planetary sciences,[12,13] glaciology and snow ductile-brittle fracture,[14] and metamorphism,[15] as well as cold region engineering.[16]

Ice sintering force can be related to the presence of a liquid layer on the ice surface.[2,17] Historically, the presence of this liquid layer was related to pressure melting, as proposed by Thompson in 1850 (see detailed description in Ref. 18), and this theory dominated the scientific society for long. The current consensus though is that the frictional heating–melting,[19] and Faraday's liquid layer freezing[20] effects are the dominant sources for the presence of this liquid layer.[21–27] Recent experimental and numerical studies provide detailed insight into the characteristics of the liquid layer formation and variation as a function of temperature and explain how the disordering of the topmost ice surface governs the slipperiness of the ice surface.[28,29]

In 1954, Jensen (see page 26 in Ref. 30) indicated via experiments that the ice sintering force decreases exponentially as the temperature drops. This exponential decrement which is in the form of the Arrhenius equation was used in ice studies to commensurate the results between different temperatures.[2,31–33] Kingery[34] measured sintering force for the ice particles in the size range of

© Author(s) 2022

0.1–3 mm generated in liquid oxygen or nitrogen. The particles were brought together "lightly" and it was shown that pressure melting is not essential for the welding of the ice particles but the surface water diffusion is. Neck radius was shown to increase with both the time and the particle size. Moreover, the temperature dependence was also found to follow an Arrhenius equation but the estimated activation energy is much higher than the value commonly acknowledged today. Gubler[35] conducted a series of measurements and obtained an ice sintering force for the initial state of sintering for time scales between 1 and 500 s. In 2003, Fan *et al.*[17] experimented micrometer-sized ice particles, which were put together gently, and measured the developed sintering force over time. The main conclusions were that ice sintering occurs even without external pressure, and that this sintering force increases with both time and particle size. In another study in 2007, Szabo and Schneebeli[2] tested two ice cones under a constant external pressure and measured the sintering force for the duration of less than a second while keeping relative humidity around 50%. They also predicted the sintering force for the same particle size when the external force varied from small to larger values. They found both experimentally and analytically that ice particles stick to each other in less than a second even when the contact load and durations are very small.

Analytically, Colbeck[36] developed a formula for the rate of bond growth based on the assumption that the bond neck is groove-shaped and obtained a closed-form solution for the force. However, the final formula is difficult to use since it depends on parameters like liquid layer thickness on the surface of ice particles which are not accurately known. A simple formulation was also developed by Szabo and Schneebeli.[2] However, their assumptions of a constant strain rate vs time for the initial sintering stage, ignoring stress concentration factor for the fracture load calculation, and application of Hertzian contact theory are questionable.

Although previous studies provide much insight into ice sintering, there are some points requiring a unified investigation. For instance, in the work of Fan *et al.*,[17] there was no contact force reported during the sintering, while in the work of Szabo and Schneebeli,[2] there was no particle size variation. A study that considers all relevant variables experimentally and provides a simple and applied theoretical framework is lacking in the literature.

In this study, we, therefore, investigate the ice sintering, and we find experimentally that (1) the sintering force is a strong function of temperature, size, contact load, and contact duration, (2) for fast sintering, the sintering force takes on small values. We also utilize existing strain-rate data from the literature and obtain an analytical formulation that predicts the observed forces for different contact loads, durations, sizes, and temperatures.

II. METHODS

A. Experimental setup

The experiments are phenomenologically presented in Fig. 1. Two ice particles of radii r and R, respectively, are pressed against each other by a force $F(t)$ during a given temporal duration, t_f. A typical force history is indicated in Fig. 1(b). As a result of the contact, the contact radius will grow to a final size a_f and the corresponding bonding force F_{sint} is measured as the force needed to break up the bond.

The equipment used for the experiments is shown in Fig. 2. We use a freezer with minimum achievable temperature of around −20 °C as climate chamber and control the temperature in the freezer using a PID (proportional integral derivative) controller (Shinko JCD series). The experimental equipment is installed on a rigid base and is located on a base in the freezer. Variations of the temperature inside the freezer are logged into a computer file using SignalExpress software (National Instruments, version 2015) over night with a sampling rate of 1 per 25 s. The variation in the temperature throughout the experiments is found to be less than ±0.75 °C. The humidity of the freezer is kept around 50% for all the experiments. The force profile, F, depicted in Fig. 1(b), can be formulated as a function of time, t,

$$F(t) = \begin{cases} \left(\frac{t}{t_{load}}\right) F_{max}; & t < t_{load}, \\ F_{max}\ ; & t_{load} \le t < t_{load} + t_{keep}, \\ \left(\frac{t_f - t}{t_{unload}}\right) F_{max}; & t_{load} + t_{keep} \le t \le t_f, \end{cases} \quad (1)$$

where F_{max} is the maximum imposed force and t_{load} and t_f are the loading and contact durations, as depicted in Fig. 1(b), respectively.

To measure the temperature inside the freezer, we use a thermometer (type Testo 400, Testo Inc.) which is equipped with a hygrometer and can send data to a wireless screen using Bluetooth technology. The temperature probe from the thermometer is at approximately 1 cm from the ice samples and in the same height or z value.

To measure the sintering force, we use a FUTEK LSB200 load-cell (FUTEK, Advanced sensor technology Inc.) with capacity of 0.1 N. The sampling rate of the measurements is 50 samples per second. The load cell is calibrated with precise weights and the reading of the load cell is temperature compensated. We use a linear servo controller (E625 series, Physik instrumente) to actuate the load cell via LabVIEW (National instruments) commands through an in-house LabVIEW (National instruments) program. The force and displacement values as a function of time are saved on the computer.

To enable easy unmounting of the ice particle from the load-cell, we utilize the body of a vaccine tube and glue it to the plate of the load cell, as presented in Fig. 2(b). The hollow cap of the vaccine tube (internal diameter 10 mm) is used as a mold to create an ice particle and to fasten/unfasten it to the tube easily. This procedure results in a spherical ice cap of fixed radius, $R = 5.0$ mm mounted on the load cell. The other ice particle is created using a water droplet attached to the tip of a syringe. The syringe itself is put in vertical direction upside down on top of the ice particle on the vaccine cap. De-ionized water is used to create both ice samples. Different syringe tip sizes are used to obtain different particle sizes for the top spherical ice particles in the radius size range from 0.6 to 2 mm. Both the load cell and the holder holding the syringe are mounted on translation stages to enable fine tuning of the position in independent Cartesian directions (x–y–z) to have the ice particles contacting in an aligned manner.

© Author(s) 2022

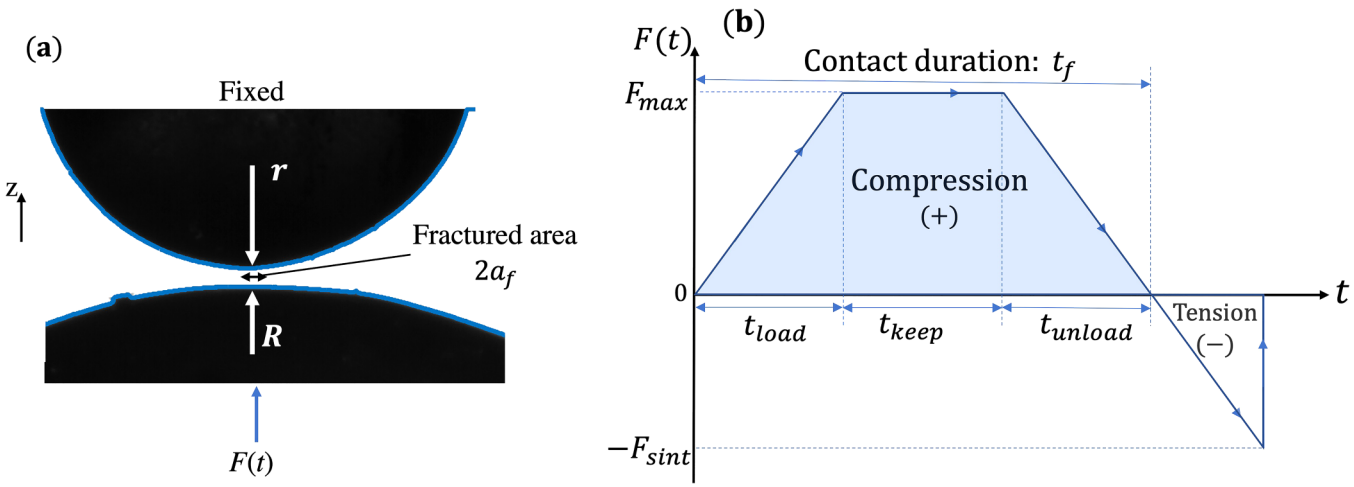

FIG. 1. (a) A typical fracture area for a specific experiment: $r = 1.2$ mm; $R = 5$ mm; and $2a_f = 0.15$ mm (b) Idealized loading history used in the analytic calculations. Compression loads are considered as positive and tensile loads as negative, respectively.

We employ two cameras. The main camera (IDS uEye UI-314× series, 1280 × 1024 resolution, IDS Imaging Development Systems GmbH) and an auxiliary camera (IDS uEye UI-324× series, 1280 × 1024 resolution, IDS Imaging Development Systems GmbH) are used in two perpendicular Cartesian directions (x–y) to trace the movement and deformation of the ice particles. The main camera is equipped with a telecentric lens (fixed magnification, $m = 1$) to record one-to-one images and is used for analysis purposes. In this view, the images are acquired in diffuse back-illumination from a LED light source. The auxiliary camera is mainly used for visualization purposes and also to help adjusting the initial relative location of ice particles and ice bed to ensure alignment of the tips.

To measure the radius of the particles, we use a MATLAB (R2021a, Mathworks Inc, Natick, Massachusetts) program. For each particle, two images in x and y directions, from the main and auxiliary cameras, are considered, respectively. We manually crop the images to a region near the contact point, detect the boundary

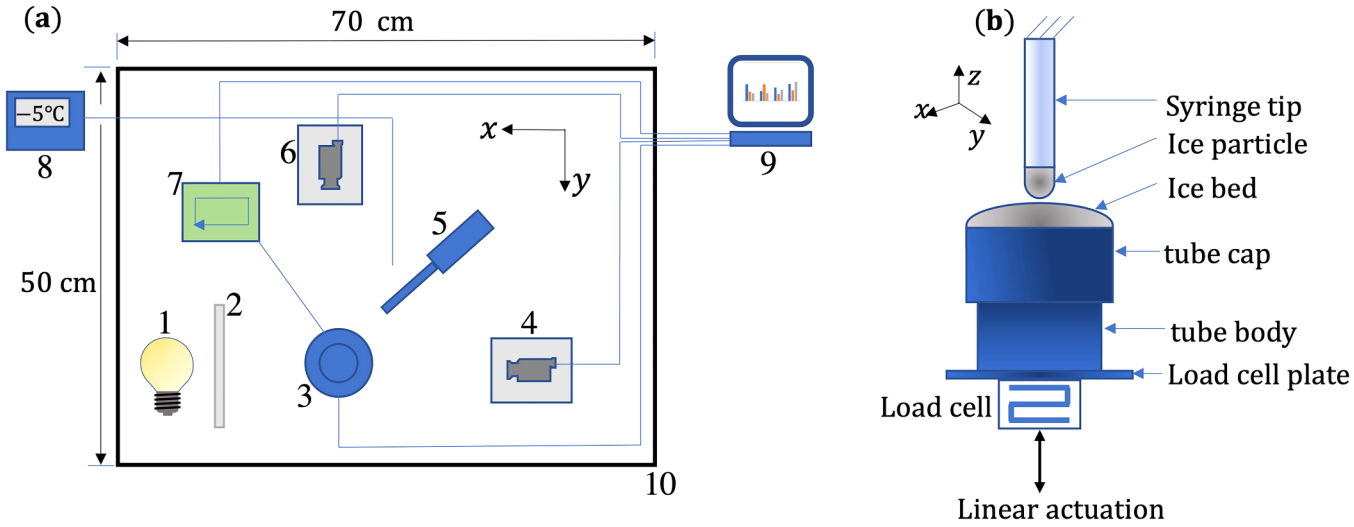

FIG. 2. (a) Experimental setup: 1—LED light source, 2—diffuser plate, 3—syringe for top ice particles and load cell and holder for bottom ice particle, 4—main camera, 5—bluetooth thermometer and humidity indicator, 6—auxiliary camera, 7—servo controller, 8—PID controller, 9—computer, and 10—freezer (dimensions in x, y, and z directions are 70, 60, and 70 cm, respectively) and (b) the details of item 3.

© Author(s) 2022

automatically, and use a least-square circle-fitting to the boundary to find the radii r and R of the fitted circles. A typical image from the main camera is depicted in Fig. 1(a), and the detected boundary is shown by the blue curve on it. The bond width associated with the fracture region is obtained by manual pixel counting.

The idealized profile of the imposed contact load on the particles is presented schematically in Fig. 1(b). A linear loading and unloading constitutes the initial and final stages, and a middle stage holding (or keeping) is used to press the particles together under a constant load. The loading starts at time zero from no force condition and monotonically continues to a maximum force, F_{max}, during a time t_{load}. Then, the force is kept at F_{max} for a duration of t_{keep}. Finally, the load is monotonically decreased to a no force state during a time t_{unload}. The time $t_f = t_{load} + t_{keep} + t_{unload}$ is considered to be the contact time. The loading continues in the tensile direction until the bond between the particles breaks. The force, thus, registered is considered to be the sintering force, F_{sint}.

An overview of the various experiments conducted in this study is presented in Table I. In total, 16 experiments with different settings are conducted, and each experiment is repeated five times. In the table, the loading histories TS1 and TS2 require some clarification. During the experiments, a constant loading rate was utilized and to account for variations in $F_{\max}$, t_{load}, and t_{unload} are scaled in relation to the maximum force expressed in mN. Hence, the loading time for a maximum force of 10 mN becomes 21 s. In addition, values within {} brackets represent a set of settings with otherwise constant values.

B. Analytical formulation

The particle model used to derive the analytic relation is shown in Fig. 1(a). A spherical ice particle of radius, r, is pressed against another spherical ice particle of radius, R, under the compressive force $F(t)$. Because of the compression, the particles are in contact in a circular area of size $A_c(t) = \pi a^2(t)$, where $a(t)$ is the radius of the contact area. With reference to Fig. 1(b), the bond is assumed to grow throughout the entire compression phase of the loading cycle giving a remaining sintering force,

$$F_{sint}(T, F, R^*, t_f) = \pi e^k \left(\frac{S_{ut}}{K_s}\right) a^2(F, R^*, t_f), \tag{2}$$

at the end of the loading cycle where $t_f = t_{load} + t_{keep} + t_{unload}$ is the total loading time. Equation (2) is grounded at $T = -5$ °C. The reason for this choice is that experimental data for this temperature is provided by Mellor and Cole that is used to model the strain response of ice, see Eq. (6).[37,38] In addition, the temperature dependence of ice has previously been shown to be well described by an Arrhenius type of equation.[31] The temperature dependence is, therefore, modeled as e^k, where

$$k = -\frac{Q}{nR_g}\left(\frac{1}{273.15 + T} - \frac{1}{268.15}\right) \tag{3}$$

is the exponent of the Arrhenius equation. In Eq. (2), $Q = 133$ kJ/mol,[39] $n = 3$, and $R_g = 8.314$ J/K mol is the molar gas constant.[16] In addition, the temperature T is given in °C in and the reference temperature 268.15 K is included. The strength of the bond is scaled according to S_{ut}/K_s, where S_{ut} is the ultimate strength of ice[40] and K_s is the axial stress concentration factor for the contact. As an exact value of the stress concentration factor is difficult to predict for the contacts considered, S_{ut}/K_s will be treated as a tuning factor to adjust the level of the measured sintering force with experimental results. In fact, a value of $S_{ut}/K_s = 1.1$ MPa was found to provide a good fit in all the experiments, see Sec. III. The time evolution of the contact radius $a(t)$ is modeled in accordance with[41] as

$$a^2(t_1) = a_0^2 + 2R^{*2}\int_0^{t_1} \dot{\varepsilon} dt, \tag{4}$$

where $\dot{\varepsilon}$ is the strain rate, $R^* = rR/(r + R)$ is the equivalent radius, and[42]

$$a_0 = (9\pi W R^{*2}/2E^*)^{1/3} \tag{5}$$

is the contact area radius at time $t = 0$ as predicted from the Johnson–Kendall–Roberts (JKR) model.[43] $E^* = 0.5E/(1 - \nu^2)$ appearing in Eq. (5) is the effective modulus where Young's modulus of ice is taken to be $E = 9.66$ GPa[44] and Poisson's ratio $\nu = 0.32$.[16] Similarly, $W = 0.2$ N/m is the work of adhesion.[45] An estimation of the strain rate at $T = -5$ °C for the initial stage of sintering is obtained from experimental data as[37,38]

$$\dot{\varepsilon} = 5.52 \times 10^{-6}\sigma^{2.43}\alpha_s t^{-1/3}, \tag{6}$$

where σ is the contact pressure in MPa and t is time in seconds. Assuming a spherical contact, the contact pressure is modeled as[46]

$$\sigma(t) = \frac{3F(t)}{2\pi a^2(t)}, \tag{7}$$

where $F(t)$ again is the compressive force modeled in Fig. 1(b). The

TABLE I. An overview of the various experiments conducted in this study; loading history: TS1 ≡ {t_{load} = 2.1F_{max} (s), t_{keep} = 0.1 (s), t_{unload} = 2.1F_{max} (s)} and TS2 ≡ {t_{load} = 21 (s), t_{keep} = {0.1, 10, 50, 100} (s), t_{unload} = 21 (s)}.

Smaller radius, r, (mm)	Experiment: [Temperature, T, (°C); Loading history; and Load, F_{max}, (mN)]
0.61	[−12, TS1, 10]
0.65	[−12, TS1, 10]
0.75	[−12, TS1, 10]
1.20	[−2, TS1, 10], [−4, TS1, 10], [−7, TS1, 10], [−12, TS1, {1, 5, 10, 15}], [−12, TS2, 10], [−16, TS1, 10]
1.61	[−12, TS1, 10]
2.02	[−12, TS1, 10]

© Author(s) 2022

factor α_s appearing in Eq. (6) is a scaling factor that depends on the strain level, ε, according to

$$\alpha_s = \begin{cases} 5 - 4.7\varepsilon; & \varepsilon \le 0.009, \\ 4.7\varepsilon - 3; & \varepsilon > 0.009, \end{cases} \tag{8}$$

where ε was defined as

$$\varepsilon = 1 - \sqrt{R^{*2} - a^2}/R^*. \tag{9}$$

Finally, the radius of the contact area to be used in Eq. (1) is modeled as

$$a^2(F, R^*, t_f) = \left(\frac{9\pi W R^{*2}}{2E^*}\right)^{2/3} + 2.904 \times 10^{-20} R^{*2} \alpha_s \int_{t=0}^{t_f} \left[\frac{3F(t)}{2\pi a^2(t)}\right]^{2.43} t^{-1/3} dt, \tag{10}$$

where again $T = -5\ ^\circ\mathrm{C}$ is considered to be the reference temperature. Equation (6) is a class of integral equations known as a singular Volterra equation.[47] Analytic solution for Eq. (10) exists when α_s is a constant. In the general case, where α_s is not a constant and follows Eq. (8), a numerical solution is implemented with details provided in Ref. 48. Starting with an initial contact radius, Eqs. (2) and (10) are the main relations that include the history of the contact used to model the sintering force. In Sec. III, these equations are evaluated in a set of experiments as described in Sec. II A.

Assuming α_s to take on a constant value enables a close-form solution for the bond radius and sintering force to be found. With, $\alpha_s = 5$, we take derivatives of the two sides of Eq. (10), separate the variables with respect to time, t, on one side and bond radius, a, on the other side. We then integrate both sides to get

$$\int_0^{a_f} a^{1+2m}\, da = C_0 R^{*2} \int_0^{t_f} F(t) t^{-\beta} dt, \tag{11}$$

where a_f is the bond radius at the end of unloading, t_f, $C_0 = 1.204 \times 10^{-20}$, $m = 2.43$, and $\beta = 1/3$.

Evaluating the above integral, using the force profile in Eq. (1), we obtain the bond radius, a_f, as

$$a_f = \left\{ \left(\frac{9\pi W R^{*2}}{2E^*}\right)^{\frac{2(1+m)}{3}} . + 2C_0 R^{*2}(1+m) F_{max}^m \left[\frac{t_l^{1-\beta}}{1+m-\beta} + \frac{(t_l+t_k)^{1-\beta} - t_l^{1-\beta}}{1-\beta} . + \left(\frac{t_f}{t_u}\right)^{1+m-\beta} t_u^{1-\beta} \left(\mathbf{B}_1(1-\beta, 1+\alpha) - \mathbf{B}_{1-\frac{t_u}{t_f}}(1-\beta, 1+\alpha) \right) \right] \right\}^{\frac{1}{2(1+m)}}, \tag{12}$$

where $t_l \equiv t_{load}$, $t_k \equiv t_{keep}$, $t_u \equiv t_{unload}$, and $\mathbf{B}$ is the incomplete beta function defined as[49]

$$\mathbf{B}_z(a, b) = \int_0^z u^{a-1}(1-u)^{b-1} du. \tag{13}$$

The corresponding sintering force becomes

$$F_{sint} = \left(\frac{S_{ut}}{K_s}\right) \pi e^k \left\{ \left(\frac{9\pi W R^{*2}}{2E^*}\right)^{\frac{2(1+m)}{3}} . + 2C_0 R^{*2}(1+m) F_{max}^m \left[\frac{t_l^{1-\beta}}{1+m-\beta} + \frac{(t_l+t_k)^{1-\beta} - t_l^{1-\beta}}{1-\beta} . + \left(\frac{t_f}{t_u}\right)^{1+m-\beta} t_u^{1-\beta} \left(\mathbf{B}_1(1-\beta, 1+\alpha) - \mathbf{B}_{1-\frac{t_u}{t_f}}(1-\beta, 1+\alpha) \right) \right] \right\}^{\frac{1}{(1+m)}}. \tag{14}$$

As previously, the value of $\frac{S_{ut}}{K_s} = 1.1$ MPa for all the calculations. In Sec. III, the results from the close-form solution in Eqs. (12) and (14) are compared with the numerical solution, Eqs. (2) and (10), in relations to the experimental data.

III. RESULTS

A typical sample of a measured force–displacement curve is presented in Fig. 3(a). The particles start to move from a detached state, like point A, as shown in Fig. 3(a), and touch each other at point B. Then, the particles are pushed together until point C. At point C, the velocity becomes zero and the particles are kept stationary from point C to point C′, where the movement direction reverses. At point D, the particles are still touching each other but they are moving apart and the force between them is zero. After point D, the bond between the particles, which has been formed during the pressing from B to D, is stretched until it breaks at point E. The corresponding force–time curve for the same test is

© Author(s) 2022

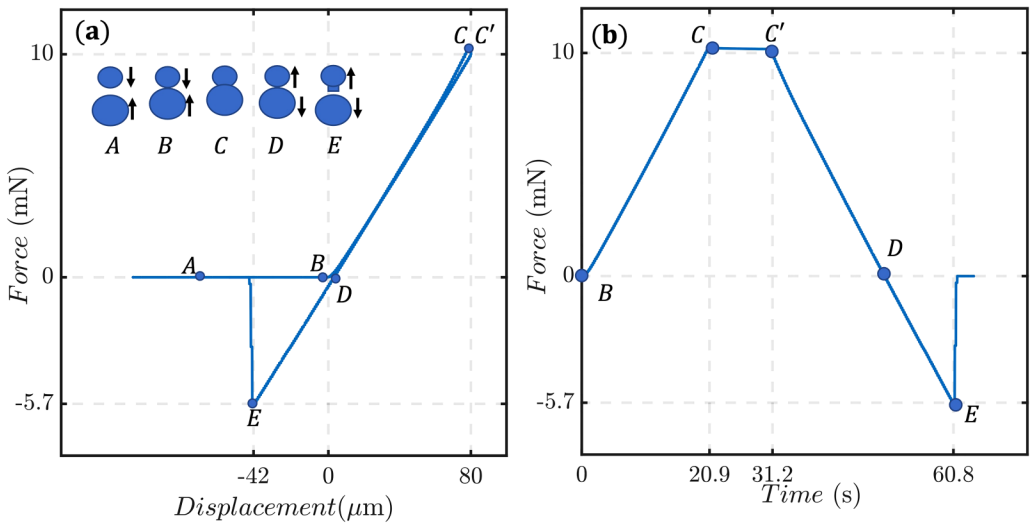

FIG. 3. (a) Sample experimental force–displacement and (b) force–time curve during one test; and plots are for $r = 1.2$ mm; $R \approx 5$ mm; $T = -12$ °C when the applied contact load is $F_{max} = 10$ mN. The observed sintering force is around 5.7 mN. Note that the positive force indicates compression, and the negative force indicates tension.

depicted in Fig. (3)(b), where the loading and unloading phases are almost linear as idealized in Fig. 1(b). Visibly, the fracture is almost brittle, and the force value drops rapidly from the sintering force, 5.7 mN, to zero. In the following, experimental and analytical results for sintering force are presented when the contact load, duration, particle size, or temperature is varied, respectively. The experimental results are taken from the experiments summarized in Table I, and the analytical results are sampled from Eqs. (1) and (8), respectively, and connected by a fitting equation. In addition, a verification of the analytic model for previously published experimental results from fast sintering of ice is presented. Finally, the development of the sintering force and the bond diameter as a function of time are discussed based on the analytic model.

A. Contact load

Results for the sintering force as a function of maximum contact load are presented in Fig. 4. The experiments utilized are summarized on the fourth line and fourth set in Table I. Hence, the temperature $T = -12$ °C, the radius of the smaller ice particle is $r = 1.2$ mm, and the radius of the ice bed is $R \approx 5$ mm. In addition, the keep time $t_{keep} = 0.1$ s and $t_{load}(s) = t_{unload}(s) = 2.1F_{max}(\text{mN})$ for all the measurements. The maximum contact force varied between 1 and 15 mN. In agreement with previous measurements,[2] we find a nearly linear dependence between the sintering force and the applied contact load.

B. Contact durations

The variation of the measured sintering force as a function, the contact duration, t_f, is presented in Fig. 5. The experiments utilized are presented with loading history TS2 in Table I. Hence, the temperature $T = -12$ °C, the radius of the smaller ice particle is $r = 1.2$ mm, and the radius of the ice bed is $R \approx 5$ mm for all measurements while the keep time is varied between 0.1 and 100 s. In accordance with previous studies,[2,35] the sintering force shows a

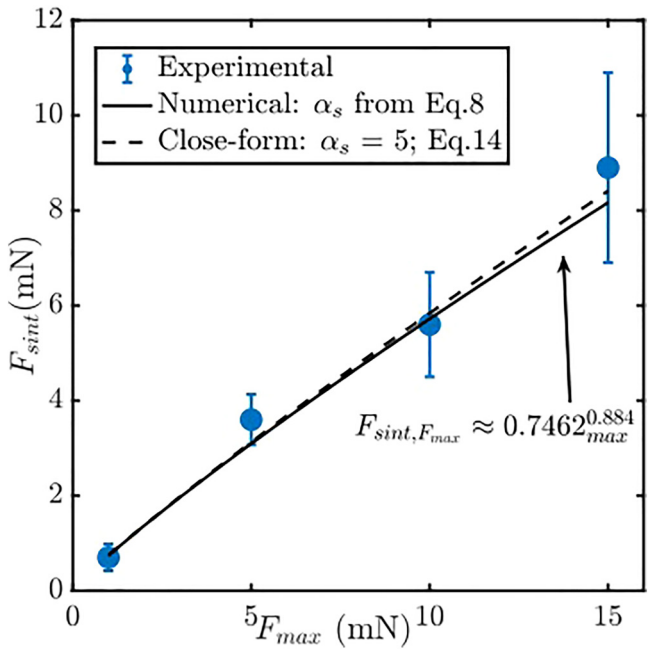

FIG. 4. Experimental and analytic sintering force as a function of particle contact load. The experimental results represent mean value ± standard deviation. Analytic results are obtained from Eq. (2).

© Author(s) 2022

nonlinear behavior that best can be described as a power law. For shorter times, the rate of growth of the sintering force is high but it slows down with the passage of time and may eventually reach a steady-state value.

C. Particle size (radius)

The dependence of the measured sintering force on the particle size is shown in Fig. 6. The results are obtained for the case where the applied contact load is $F_{max} = 10$ mN, loading and unloading times t_{load} and t_{unload} are both equal to 21 s, $t_{keep} = 0.1$ s, and the measurements were performed at $T = -12$ °C. The radius of the ice bed is $R \approx 5$ mm while the radius of the smaller particle varied between 0.61 and 2.02 mm. The different experiments are summarized in Table I as all settings written as [−12, TS1, 10]. We observed that the sintering force is larger for larger particles. In fact, the dependence of the analytical prediction for the sintering force as a function of the equivalent particle radius can be approximated by a power law function, $F_{sint} \approx 5.78R^{*0.64}$. The exponent of the power law for the size dependence is around the value predicted by general sintering theory, which is 2/3.[50]

It might be of interest here to describe the relative force, a particle "feels" compared to its own weight. While the bond force increases with $R^{0.64}$, the particle weight, w, increases with R^3, which means that the overall bond strength compared to the weight of the particle will drastically increase for smaller particles and small particles will behave much more sticky than large particles upon colliding to the surfaces. This observation is in line with previous studies that larger ice particles are less likely to adhere than smaller ones.[51]

D. Temperature

The dependence of the measured sintering force on temperature is presented in Fig. 7. The results are obtained for the case where the applied contact load is $F_{max} = 10$ mN, loading and unloading times t_{load} and t_{unload} are both equal to 21 s, and $t_{keep} = 0.1$ s. The radius of the smaller ice particle is $r = 1.2$, and the radius of ice bed is $R \approx 5$ mm. The experiments are summarized on the fourth line in Table I. Since there is no thermometer inside the ice particles, we waited for around 1 h for each ice particle to freeze and reach the expected temperature of the test. In accordance with the Arrhenius-like dependence of the sintering force on temperature assumed for the analytic approach, the matching of experimental results to the Arrhenius equation shows that it is a viable assumption.

To verify the activation energy of the contact, the experimental observations from Fig. 7 are replotted in Fig. 8 as a function of temperature in Kelvin. The obtained fitted force is found to be proportional to $\exp(-4979/T)$, with T in Kelvin. Comparing this relation by the general relation $\exp\left(-\frac{Q}{R_g T}\right)$, and considering the gas constant $R_g = 8.3145\ \frac{\text{J}}{\text{mol-K}}$, we conclude that the activation energy, $\Delta E \approx 41.4$ KJ/mol. This value is close to previously reported data, $\Delta E = Q/n = 44.3$ KJ/mol in Ref. 52.

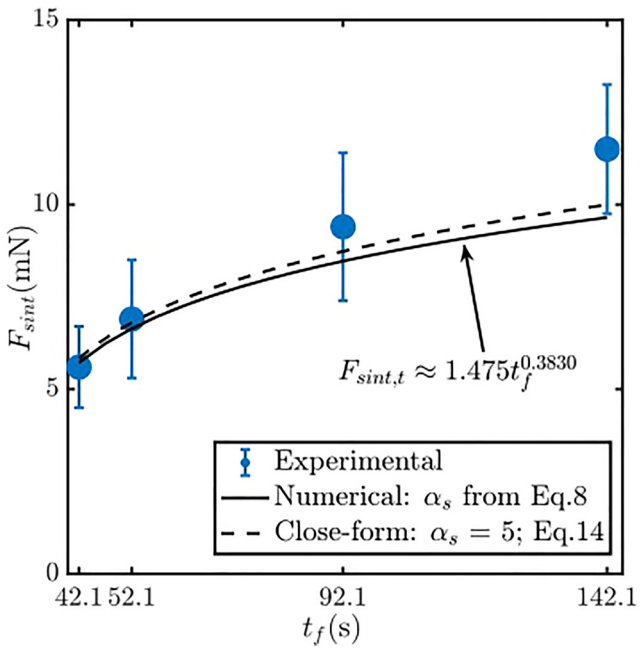

FIG. 5. Experimental and analytic sintering force as a function of contact duration. The experimental results represent mean value ± standard deviation. Analytic results are obtained from Eq. (2).

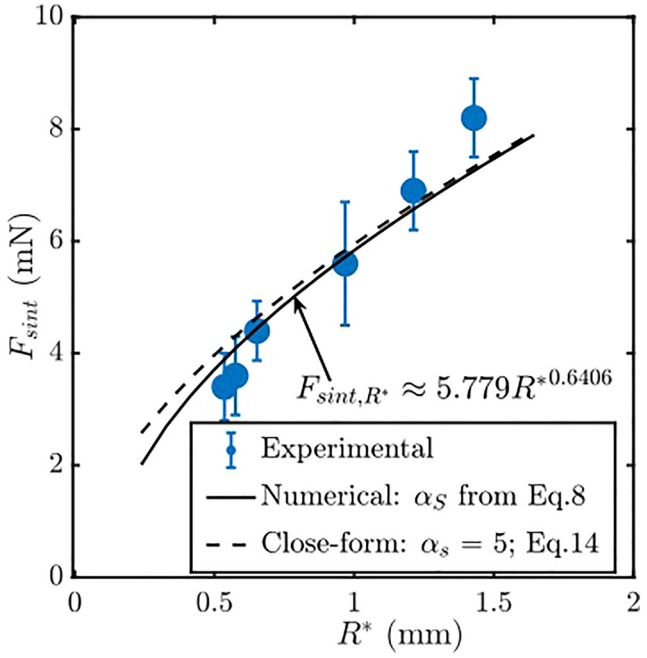

FIG. 6. Experimental and analytic sintering force as a function of equivalent radius. The experimental results represent mean value ± standard deviation. Analytic results are obtained from Eq. (2).

© Author(s) 2022

E. Fast sintering

Fast sintering of ice is of interest since it is useful in simulations dealing with collisions of ice particles. To further verify the analytic method for the case of fast sintering of ice, we compared our analytic results with experimental result obtained for sub-second sintering of ice by Szabo and Schneebeli,[2] as depicted in Fig. 9. The results are obtained for the case where $F_{max} = 2$ N and $R = r = 3$ mm. These results indicate that our analytic model can capture fast sintering of ice particles loaded for a larger force of 2 N.

F. Analytic results for bond and sintering force growth with time

The time development of the pull-off force and the bond diameter, obtained from Eqs. (1) and (8), respectively, are shown in Figs. 10(a) and 10(b). The maximum value of the pull-off force at the end of unloading, t_f, is termed as F_{sint}. The parameters used in the simulation are $T = -12°C$, $r = 1.2$ mm, $R = 5$ mm, and $F_{max} = 10$ mN. The loading history assumed is sketched in Fig. 1(b) with loading and unloading times set to 21 s and the keep time, t_{keep}, set to 10 s. As expected, both the bond diameter and the sintering force increase with time but in a nonlinear way. The main development of the bond radius and the sintering force occurs during the loading and holding (keeping) stage while the growth is almost negligible during the unloading phase. We may, therefore, conclude that for the loading cycle considered the dominant growth of the bond appears during the initial stages of the contact.

IV. DISCUSSION AND CONCLUSION

The sintering force given by Eq. (14) and the corresponding contact radius given by Eq. (12) are the main results from this paper. These equations are shown to depend on the force history, contact time, and the equivalent radius in a rather complex way described by an integral equation. In addition, it was verified that the scaling of the sintering force with respect to temperature is sufficiently described by the Arrhenius equation. The relations were further verified for a few experiments characterized by a linear force ramp-up and ramp-down, respectively, with a constant force keep time in between. For these experiments, the relation between applied contact load and sintering force is nearly linear with a slope of roughly 0.75. Hence, if the contact force is doubled the sintering force becomes 50% stronger if all other parameters are kept constant. In contrast, the relation between the sintering force and the equivalent radius tends to follow a power law with an exponent of roughly 0.64, which is close to the value 2/3 predicted by general sintering theory.[50] The relative value of bond strength to particle weight, which changes with cubic radius, is then much larger as the particles become smaller and smaller particles tend to stick easier than the larger particles, as suggested in previous studies.[51] The relation between the measured sintering force and the contact duration appears to follow a power law with an exponent in the order

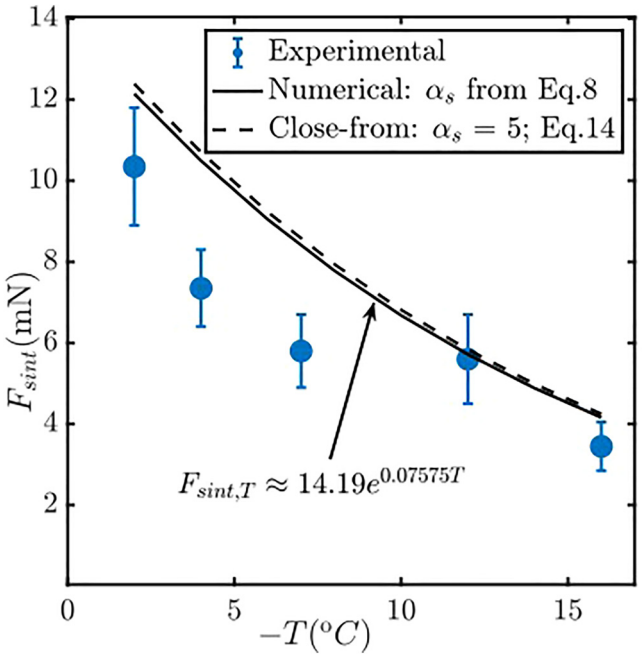

FIG. 7. Experimental and analytic sintering force as a function of temperature. The experimental results represent mean value ± standard deviation. Analytic results are obtained from Eq. (2).

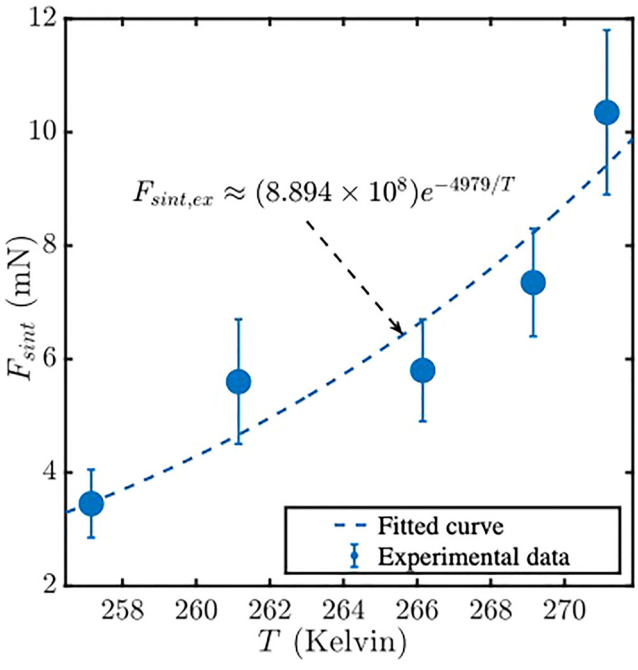

FIG. 8. Experimental values of the measured sintering force at different temperatures and the curve fitted to the mean value points. The experimental results represent mean value ± standard deviation.

© Author(s) 2022

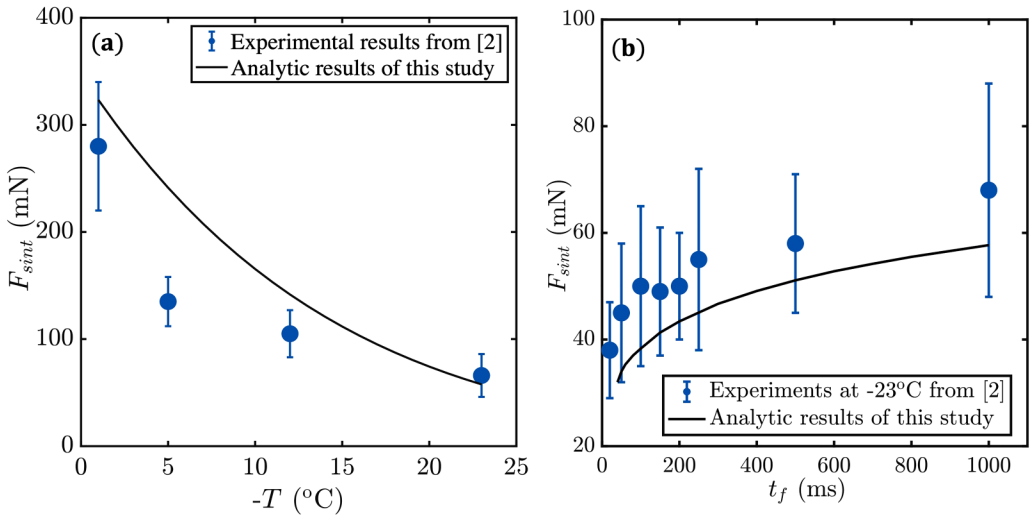

FIG. 9. Experimental sintering force extracted from Szabo and Schneebeli,[2] and analytic sintering force predicted from this study: (a) temperature dependence while $t_{load} = t_{unload} = 495$ ms and $t_{keep} = 10$ ms, which results in $t_f = 1$ s and (b) time dependence, while t_f is varied, $t_{keep} = 10$ ms, and $t_{load} = t_{unload} = 0.5(t_f - t_{keep})$.

of 0.38. This means that initially the bond grows strong rather quickly and as the contact time increases the strength of the bond tends toward a constant value. Hence, there may be a maximum value for the bond. If such a value does exist is, however, outside the scope of this paper. On the other side, the model successfully predicts the sintering force for sub-second contact durations based on measurements previously presented in the literature.

We also obtained the activation energy using our experimental measurements for the sintering force at different temperatures. We find that the activation energy is around 41.4 KJ/mol and close to the previously reported data, $\Delta E = 44.3$ KJ/mol in Ref. 52.

As ice is a brittle material, it is of importance to acknowledge the geometry close to the contact zone for calculation of the ultimate strength of the bond, which is considered by the stress concentration factor. As the range of equivalent radii in these experiments were rather small, the stress concentration factor has been treated as a constant throughout the analysis, which resulted in the constant scaling factor $S_{ut}/K_s = 1.1$ MPa for all the

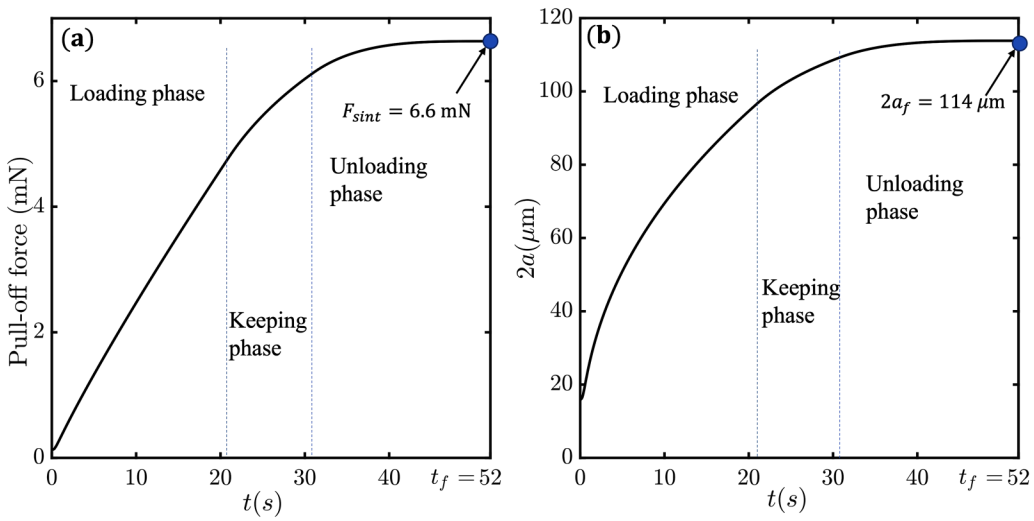

FIG. 10. Analytic results for the development of the (a) pull-off force as a function of time and (b) bond diameter $2a$ as a function of time. The sintering force becomes $F_{sint} = 6.6$ mN and the final bond radius become $a_f \approx 57$ μm. Plots are obtained for parameters $F_{max} = 10$ mN; $r = 1.2$ mm; R ≈ 5 mm; $T = -12$ °C.

© Author(s) 2022

experiments, where S_{ut} is the ultimate strength of ice and K_s is the axial stress concentration factor.

One interesting observation from the experiments is that during freezing many particles experienced cavitation and cracking similar to what has been observed in previous studies.[53] These phenomena did not lead to a macroscopic change in particle shape mainly because of the presence of the holding needle from the syringe. However, ice cracking during the formation of the particles can be one source for the observed variations in the measured forces.

The model presented in this paper has been shown to be capable of capturing the variation in the sintering force within a limited domain of equivalent radii, temperatures, contact loads, and durations, respectively. In addition, the relative humidity was kept constant at 50% all through the measurements. Despite these limitations the ranges chosen are typical for some practical problems including manufactured and stored snow, which potentially makes it a valuable model in simulations. To which degree the model changes with humidity and outside the ranges considered is an interesting topic for future investigations.

ACKNOWLEDGMENTS

We are particularly grateful to Dr. Henrik Lycksam who provided technical support in setting up several devices and methods during the experiments and assisted in acquiring the required tools and materials for the experiments. We are grateful to the anonymous reviewers for their constructive comments during the review process.

AUTHOR DECLARATIONS

Conflict of Interest

The authors have no conflicts to disclose.

DATA AVAILABILITY

The data that support the findings of this study are available from the corresponding author upon reasonable request.

REFERENCES

[1]C. Willibald, J. Dual, M. Schneebeli, and H. Löwe, "Size controls on the crossover from normal to self-inhibited sintering of ice spheres," Acta Mater. **213**, 116926 (2021).
[2]D. Szabo and M. Schneebeli, "Subsecond sintering of ice," Appl. Phys. Lett. **90**, 151916 (2007).
[3]J. R. Blackford, "Sintering and microstructure of ice: A review," J. Phys. D: Appl. Phys. **40**, R355 (2007).
[4]B. W. Kabore and B. Peters, "Micromechanical model for sintering and damage in viscoelastic porous ice and snow: Part I: Model and calibration," Int. J. Solids Struct. **185–186**, 324 (2020).
[5]B. W. Kabore and B. Peters, "Micromechanical model for sintering and damage in viscoelastic porous ice and snow: Part II: Validation," Int. J. Solids Struct. **185–186**, 281 (2020).
[6]P. Bartelt, C. V. Valero, T. Feistl, M. Christen, Y. Bühler, and O. Buser, "Modelling cohesion in snow avalanche flow," J. Glaciol. **61**, 837 (2015).
[7]N. Maeno and M. Arakawa, "Adhesion shear theory of ice friction at low sliding velocities, combined with ice sintering," J. Appl. Phys. **95**, 134 (2004).
[8]T. Eidevag, E. S. Thomson, D. Kallin, J. Casselgren, and A. Rasmuson, "Angle of repose of snow: An experimental study on cohesive properties," Cold Reg. Sci. Technol. **194**, 103470 (2021).
[9]J. Gaume, A. Van Herwijnen, G. Chambon, N. Wever, and J. Schweizer, "Snow fracture in relation to slab avalanche release: Critical state for the onset of crack propagation," Cryosphere **11**, 217 (2017).
[10]D. Mulak and J. Gaume, "Numerical investigation of the mixed-mode failure of snow," Comput. Part. Mech. **6**, 439 (2019).
[11]A. Capelli, I. Reiweger, and J. Schweizer, "Studying snow failure with fiber bundle models," Front. Phys. **8**, 236 (2020).
[12]F. G. Bridges, K. D. Supulver, D. N. C. Lin, R. Knight, and M. Zafra, "Energy loss and sticking mechanisms in particle aggregation in planetesimal formation," Icarus **123**, 422 (1996).
[13]T. Schultz, R. Müller, D. Gross, and A. Humbert, "Modelling the transformation from snow to ice based on the underlying sintering process," PAMM **20**, 2020 (2021).
[14]H. Löwe, M. Zaiser, S. Mösinger, and S. Schleef, "Snow mechanics near the ductile-brittle transition: Compressive stick-slip and snow microquakes," Geophys. Res. Lett. **47**, e2019GL085491, https://doi.org/10.1029/2019GL085491 (2020).
[15]A. V. Herwijnen and D. A. Miller, "Experimental and numerical investigation of the sintering rate of snow," J. Glaciol. **59**, 269 (2013).
[16]V. F. Petrenko and R. W. Whitworth, *Physics of Ice* (Oxford University Press, 2006).
[17]X. Fan, P. Ten, C. Clarke, A. Bramley, and Z. Zhang, "Direct measurement of the adhesive force between ice particles by micromanipulation," Powder Technol. **131**, 105 (2003).
[18]R. Rosenberg, "Why is ice slippery," Phys. Today **58**, 50 (2005).
[19]F. P. Bowden and T. P. Hughes, "The mechanism of sliding on ice and snow," Proc. R. Soc. London. Ser. A. Math. Phys. Sci. **172**, 280 (1939).
[20]M. Faraday, "On regelation, and on the conservation of force," Philos. Mag. **17**, 162 (1859).
[21]T. Theile, H. Löwe, T. C. Theile, and M. Schneebeli, "Simulating creep of snow based on microstructure and the anisotropic deformation of ice," Acta Mater. **59**, 7104 (2011).
[22]I. Einav, "Breakage mechanics—Part I: Theory," J. Mech. Phys. Solids **55**, 1274 (2007).
[23]J. L. Molaro, G. MErion-Griffith, and C. B. Phillips, "Ice sintering timescales at the surface of Europa and implications for surface strength," Lunar Planet. Sci. **549**, 40 (2017).
[24]J. M. J. van Leeuwen, "Skating on slippery ice," SciPost Phys. **3**, 042 (2017).
[25]M. Ovaska and A. J. Tuononen, "Multiscale imaging of wear tracks in ice skate friction," Tribol. Int. **121**, 280 (2018).
[26]B. Slater and A. Michaelides, "Surface premelting of water ice," Nat. Rev. Chem. **3**, 172 (2019).
[27]A. Spagni, A. Berardo, D. Marchetto, E. Gualtieri, N. M. Pugno, and S. Valeri, "Friction of rough surfaces on ice: Experiments and modeling," Wear **368–369**, 258 (2016).
[28]Y. Nagata, T. Hama, E. H. G. Backus, M. Mezger, D. Bonn, M. Bonn, and G. Sazaki, "The surface of ice under equilibrium and nonequilibrium conditions," Acc. Chem. Res. **52**, 1006 (2019).
[29]B. Weber, Y. Nagata, S. Ketzetzi, F. Tang, W. J. Smit, H. J. Bakker, E. H. G. Backus, M. Bonn, and D. Bonn, "Molecular insight into the slipperiness of Ice," J. Phys. Chem. Lett. **9**, 2838 (2018).
[30]P. V. Hobbs, *The Sintering and Adhesion of Ice* (University of London, 1963).
[31]O. S. Toker, S. Karaman, F. Yuksel, M. Dogan, A. Kayacier, and M. T. Yilmaz, "Temperature dependency of steady, dynamic, and creep-recovery rheological properties of ice cream mix," Food Bioprocess Technol. **6**, 2974 (2013).
[32]R. W. Liefferink, F. C. Hsia, B. Weber, and D. Bonn, "Friction on ice: How temperature, pressure, and speed control the slipperiness of ice," Phys. Rev. X **11**, 011025 (2021).
[33]T. Eidevåg, E. S. Thomson, S. Sollén, J. Casselgren, and A. Rasmuson, "Collisional damping of spherical ice particles," Powder Technol. **383**, 318 (2021).

© Author(s) 2022

[34]W. D. Kingery, "Regelation, surface diffusion, and ice sintering," J. Appl. Phys. **31**, 833 (1960).
[35]H. Gubler, "Strength of bonds between ice grains after short contact times," J. Glaciol. **28**, 457 (1982).
[36]S. C. Colbeck, "Sintering in a dry snow cover," J. Appl. Phys. **84**, 4585 (1998).
[37]M. Mellor and D. M. Cole, "Deformation and failure of ice under constant stress or constant strain-rate," Cold Reg. Sci. Technol. **5**, 201 (1982).
[38]F. Azizi, "Primary creep of polycrystalline ice under constant stress," Cold Reg. Sci. Technol. **16**, 159 (1989).
[39]J. W. Glen, "The creep of polycrystalline ice," Proc. R. Soc. A Math. Phys. Eng. Sci. **228**, 519 (1955).
[40]J. J. Petrovic, "Mechanical properties of ice and snow," J. Mater. Sci. **38**, 1 (2003).
[41]A. C. Fischer-Cripps, *Mechanical Engineering Series: Introduction to Contact Mechanics* (Springer, 2006).
[42]J. A. Greenwood, "Adhesion of elastic spheres," Proc. R. Soc. A Math. Phys. Eng. Sci. **453**, 1277 (1997).
[43]K. R. Shull, "Contact mechanics and the adhesion of soft solids," Mater. Sci. Eng. R **36**, 1 (2002).
[44]G. Dantl, "Die Elastischen Moduln von Eis-Einkristallen," Phys. Der Kondens. Mater. **7**, 390 (1968).
[45]J. D. Locatelli and P. V. Hobbs, "Fall speeds and masses of solid precipitation particles," J. Geophys. Res. **79**, 2185, https://doi.org/10.1029/JC079i015p02185 (1974).
[46]R. G. Budynas and J. K. Nisbett, *Shigley's Mechanical Engineering Design*, 10th ed. (McGraw-Hill Education, 2015).
[47]R. P. Agarwal and D. O'Regan, "Positive solutions to singular initial value problems with sign changing nonlinearities," Math. Comput. Model. **28**, 31 (1998).
[48]H. Bahaloo, see https://github.com/Bahaloo/SinteringForceForIce/blob/main/BondGrowth_rev2.m~ for "Matlab Code for Sintering Force of Ice."
[49]K. Pearson, E. S. Pearson, and N. L. Johnson, *Tables of the Incomplete Beta Function*, 2nd ed. (Cambridge University Press, 1968).
[50]S.-J. L. Kang, *Sintering -Densification, Grain Growth, and Microstructure* (Elsevier Butterworth-Heinemann, Burlington, MA, 2005).
[51]T. Eidevåg, P. Abrahamsson, M. Eng, and A. Rasmuson, "Modelling of dry snow adhesion during normal impact with surfaces," Powder Technol. **361**, 1081 (2020).
[52]H. H. G. Jellinek, "Liquid-like (transition) layer on ice," J. Colloid Interface Sci. **25**, 192 (1967).
[53]S. Wildeman, S. Sterl, C. Sun, and D. Lohse, "Fast dynamics of water droplets freezing from the outside in," Phys. Rev. Lett. **118**, 1 (2017).

© Author(s) 2022